Appl. Phys. B 66, 645–651 (1998)

Applied Physics B
Lasers
and Optics

Energy transfer in the $A^2\Sigma^+$ state of OH following $v' = 1$ excitation in a low pressure CH_4/O_2-flame

P. Monkhouse*, **S. Selle****

Physikalisch-Chemisches Institut, Im Neuenheimer Feld 253, D-69120 Heidelberg, Germany
(Fax: +49-6221/544255, E-mail: d63@ix.urz.uni-heidelberg.de)

Received: 3 February 1997/Revised version: 3 September 1997

Abstract. Using temporally, spectrally and spatially resolved laser induced fluorescence (LIF), collision-induced energy transfer was studied in the $A^2\Sigma^+(v' = 1)$ level of OH. Measurements were performed in a laminar premixed flame at 10 Torr total pressure. The low pressure allowed the spatial variation of the effective quenching rate to be determined through the flame front. In addition, the dependence of the quenching rate on rotational quantum number was measured by exciting a series of rotational lines in the range $N' = 0$–16. The results show that the total quenching rate decreases only 17% through the flame front, in the region where OH can be detected. Nevertheless, the *absolute* value of the quenching rate Q is required if absolute concentrations are to be determined from LIF-signals. The variation both of Q and of the rotational relaxation rate with excited rotational quantum state must be known for quantification of LIF-temperature measurements via the Boltzmann relation. Finally, the rotational and vibrational energy transfer (RET, VET), was investigated by recording the spectrally and temporally resolved fluorescence. For all excited rotational lines, efficient RET to neighbouring rotational states was observed, but only very little VET. Total RET rates were determined from the difference between the time-resolved broadband (total fluorescence) and narrowband (fluorescence from the laser excited level) curves. The experimental results were compared with simulations using a dynamic model, which describes the energy transfer for flame conditions. With the available input data (temperature, major species concentrations and collision-partner specific RET cross sections), good agreement was obtained.

PACS: 34.00

The OH radical has often been used as an indicator of chemical kinetics and hence of the progress of combustion. It is readily detected by laser induced fluorescence (LIF) following excitation in the UV. Temperature and concentration data derived from LIF measurements may be used as input for modelling of reactive flows for the optimisation of combustion processes. However, specific requirements of quantitativeness are placed on these data. To interpret measured LIF signals quantitatively, detailed information about quenching and relaxation (rotational, vibrational) effects caused by collisions with gases in the flame environment is needed. To study such effects, a well-characterised "model" flame is desirable; in the past, collisional processes, both on OH as well as other species, were investigated using a variety of model burners at atmospheric [1–12] and at low pressures [13–19]. However, time constants at atmospheric pressure are on the order of nanoseconds or less, so that their direct measurement requires excitation by a picosecond laser and ultrafast detection (e.g. streak camera). Also, with the exception of certain types of slot burner [3, 8], the flame front region cannot readily be investigated at atmospheric pressure. In this work a low pressure, premixed laminar flame at 10 Torr was selected, so that energy transfer processes could be studied with good spatial resolution through the flame front and using standard nanosecond laser technology.

The effects of energy transfer on LIF signals following excitation of OH $A^2\Sigma^+$ have been studied under a variety of conditions (temperature, pressure, gas composition). Most of the investigations on quenching so far in flames concerned the $v' = 0$ level [1–3, 5, 14–17], much less information is available for other levels ($v' = 1$–3) of OH [1, 4, 10–13]. Comparatively little information is available on vibrational and rotational relaxation under flame conditions [10, 12, 19–21]. Quenching and relaxation compete in any realistic environment, and, in addition, relaxation processes lead to redistribution of the populations of the laser-coupled levels, which in turn may affect the effective quenching rates. Therefore it is paramount that quenching be investigated in conjunction with rotational- and vibrational energy transfer (RET, VET). A suitable method for determining rotational relaxation rates in association with quenching rates was reported in the work of Lee et al. [15]. Their studies were performed

* Corresponding author
** *Present address*: Interdisziplinäres Zentrum für Wissenschaftliches Rechnen (IWR), Universität Heidelberg, Im Neuenheimer Feld 368, D-69120 Heidelberg, Germany

on OH ($v' = 0$) in H_2/O_2/He-flames at 19 Torr and 1300 K. These authors developed a dynamic kinetic model [15, 16] and used collision partner-specific collisional data [21, 22] to simulate the results. Furthermore, the applicability of this model to energy transfer in a wide variety of combustion environments was demonstrated [23] by applying it to simulate spectra from the literature. Very recently, further experimental and modelling (using the kinetic model of [15, 16]) work was performed [24] to assess the role of vibrational relaxation in H_2/O_2-flames containing He or N_2, respectively.

With a view to progressing towards flames of more technical interest, we apply the method of Lee et al. to a more complex flame, CH_4/O_2. This flame has a greater number of collision partners but is well characterised [18] and has been modelled [25], so that species profiles are available for simulation of experimental results. We also chose to excite OH $A^2\Sigma^+$ ($v' = 1$), since fewer data are available for this level, particularly at flame temperatures.

The stages of the work can be defined as follows: (1) time-resolved, broadband fluorescence was recorded to determine the dependence of quenching rate on rotational quantum number and on position in the flame; (2) rotationally resolved fluorescence spectra were scanned to gain a qualitative impression of the extent of RET and VET on excitation of various rotational transitions; (3) time-resolved narrowband fluorescence was recorded. From the difference of the two transients determined in (1) and (3) the corresponding total RET-rate was derived.

1 Principles of the dynamic kinetic model

The results are interpreted on the basis of a multi-level model for the case of linear LIF, in which the ground state is treated as a two-level system (laser-coupled state x and bath level X). The bath level is populated by quenching from the excited (A) state and it is assumed that no transfer from X to the laser-coupled level occurs. Only the upper (excited level) is modelled in detail. The temporal behaviour of the laser excited level l, the upper level j populated by RET and the ground state levels x and X is described by a set of differential equations:

$$\frac{\mathrm{d}n_l}{\mathrm{d}t} = (B_{xl}n_x - B_{lx}n_l)G_\nu I_\mathrm{L}(t) + \sum_{j\neq l} R_{jl}n_j - \left(\sum_{j\neq l} R_{lj} + Q_l + A_l\right) n_l \tag{1}$$

$$\frac{\mathrm{d}n_j}{\mathrm{d}t} = \sum_{j\neq l} R_{ij}n_i - \left(\sum_{j\neq l} R_{ji} + Q_j + A_j\right) n_j \tag{2}$$

$$\frac{\mathrm{d}n_x}{\mathrm{d}t} = \sum_j (Q_j + A_j)n_j \tag{3}$$

$$\frac{\mathrm{d}n_x}{\mathrm{d}t} = -(B_{xl}n_x - B_{xl}n_l)G_\nu I_\mathrm{L}(t)\,. \tag{4}$$

$R_{ij}(\mathrm{s}^{-1})$ represent the state specific transfer rates for rotational relaxation from level $i \rightarrow j$, $Q_j(\mathrm{s}^{-1})$ and $A_j(\mathrm{s}^{-1})$ are the quenching rates and the Einstein coefficients for spontaneous emission, respectively, and B_{xl}, B_{lx} are the Einstein coefficients for absorption and stimulated emission. I_L is the laser intensity and G_ν the spectral overlap integral, which represents the overlap between absorption and laser line profiles. The temporal form of the laser pulse is described by the expression:

$$I_\mathrm{L}(t) \propto t^a \exp(-bt)\,. \tag{5}$$

The quenching and RET-rates are each given by the product sum of the collision partner specific coefficients k_{ji}^R and particle number densities n_M:

$$R_{ij} = \sum_M k_{ji}^R(M)n_M; \qquad Q_j = \sum_M k_j^Q(M)n_M\,. \tag{6}$$

The number densities n_M required to calculate R_{ij} and Q_j are themselves calculated from the total flame pressure, the local temperature and the mole fractions of the corresponding collision partners. The local temperature was measured for our experimental conditions and the species mole fractions were taken from a model calculation [25]. Values for k_j^Q were calculated from the empirical expression

$$k_{N'}^Q = k_0^Q \mathrm{e}^{-\gamma N'} \tag{7}$$

whereby k_0^Q is the quenching rate coefficient for $N' = 0$ in the excited state. This expression has been shown [15] to give a better fit at flame temperatures than that using $N'(N'+1)$ in the exponent [26]. Quenching data from [21] and those recommended therein were used.

The collision partner specific k_{ji}^R coefficients for RET were calculated using data based on those of [22], parameterised using the ECS-EP (energy sudden corrected-exponential power) law [16].

Modelling of the population of a set of energy levels is performed in two stages: (1) calculation of the energy transfer rates after parameterisation of the collisional data, as described above; (2) solution of the differential equation system to calculate the time-dependence of the level populations. The measured fluorescence spectra can also be modelled, using the known spectral line form.

2 Experimental

All measurements were performed in laminar premixed CH_4/O_2 flames, stabilised on a low pressure burner. The burner head was home-built and contained a water-cooled, fine-pore stainless steel sinter plate (effective diameter 55 mm; thickness 25 mm). This ensured a homogenous flow of the premixed CH_4/O_2-gases into the burner chamber. During combustion a laminar flame propagated which could be considered one-dimensional. The burner head was mounted so that the flame propagated downwards and could be moved vertically in steps of 0.01 mm over a total distance of 50 mm using a step-motor. In this way, measurements through the flame front and burnt gas were performed.

Gas flows were regulated using mass flow controllers and were set at 1 l/min CH_4 and 2 l/min O_2, i.e. in stoichiometric ratio. The burnt gases were pumped away by a vacuum

pump. The total pressure in the burner chamber was measured by two calibrated capacitative membrane manometers (for the regions 0–10 Torr and 0–1000 Torr). The second manometer measured the pressure at 100 Torr, required during ignition of the $CH_4/O_2/N_2$ mixture. (Nitrogen served as buffer gas until ignition, but was then turned off.)

Measurements were made with an excimer laser pumped dye laser (Lambda Physik Scanmate 2E) at repetition rates of 5–10 Hz. The dye used was Coumarin 153 in Methanol. The narrow band oscillator beam, freed from ASE, then passed a Béthune cell as main amplifier. The Béthune cell ensures a high quality beam profile with low divergence. The dye laser was controlled by a LAN (Local Area Network)-Interface from a laptop. UV-Wavelengths were obtained using a frequency doubling unit with a β-barium borate crystal (BBO-I) and a beam separator. The energy of the doubled beam was 0.2 to 0.8 mJ in the region 282–283 nm, the spectral width was 0.1 cm^{-1} for this dye. This gave a spectral power density entering the burner in the range 0.15–0.60 $MW/(cm^2\,cm^{-1})$.

Four suprasil-I-quartz windows allowed optical access to the burner chamber. Fluorescence light was detected with two UV-sensitive photomultipliers (PMT), whose quantum yield was constant in the region of fluorescence (305–325 nm) studied. One PMT served for detection of the total (broadband) fluorescence, the other for detection of single rotational levels. The spectral resolution required was obtained using a monochromator (CVI DK 480, $f = 480$ mm). A grating with 2400 lines/mm and a transmission maximum of 68% at 260 nm was selected. The dispersion was 0.8 nm/mm. The desired wavelength region around the central wavelength was selected using movable slits (10–2000 μm width at a fixed height of 20 mm).

The complete set-up is shown in Fig. 1. The beam path of both the excitation and fluorescence light lay in one plane. At right angles to this plane, the distance of the beam from the burner head and hence of the measurement area in the flame could be varied. About 8% of the laser energy was coupled out and detected by a calibrated pyroelectric detector.

The size of the main laser beam was narrowed by a pinhole and made parallel using two lenses of diameter 0.2 mm. The sampled volume in the burner chamber was imaged onto the monochromator slit or PMT2, respectively, using a focussing lens. A combination of filters (transmission > 30% in the range 290–410 nm) suppressed laser stray light at 282 nm.

Each of the signals obtained was sent to a boxcar-integrator for integration with the desired time gate. Gate times of 20 ns were chosen to discriminate against the flame emission. The integrated signals were then read out to an A/D-converter. The temporal behaviour of the fluorescence signal could also be displayed on an oscilloscope and transferred as an (x, y)-diagram to the computer. In this way effective lifetimes of excited OH radicals were measured. For the lifetime measurements, 200 single-shot curves were averaged.

During recording of spectra, the laser energy arriving in the measurement volume was recorded simultaneously with the fluorescence signal. Signals from 10 shots were averaged for each measurement point. If the standard deviation was greater than 10%, the point was repeated. After the measurement, the signal intensity was normalised with the laser energy.

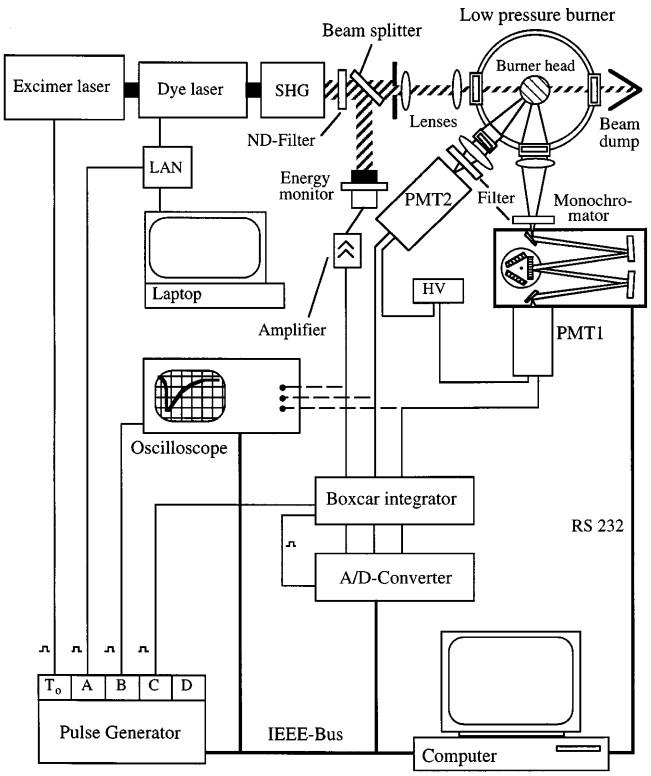

Fig. 1. Experimental set-up for LIF (broad- and narrowband detection)

3 Results and discussion

3.1 Total quenching rates as a function of position in the flame and excited rotational quantum number

The effective total lifetimes for OH $A^2\Sigma^+(v' = 1)$ following excitation of the $P_1 1$, $Q_1 3$ and $Q_1 5$ transitions were determined at heights of 2–30 mm above the burner head. Longer lifetimes (> 40 ns) were initially determined without deconvolution of the decay curves, but as a check, some measurements were deconvolved from the laser pulse using an iterative procedure (Marquardt-Algorithm). At heights of 2, 3 and 30 mm, our own temperature measurements (from excitation spectra) were available, while at the other heights, temperatures were taken from the profile of [18]. The temperatures from [18] were in good agreement with our temperatures at the relevant positions in the flame. Using these results, a temperature could be assigned to each height. Then, from each series of lifetime measurements ($\tau_{N'} = 1/(A_{N'} + Q_{N'})$ the quenching rate Q_0 for $N' = 0$ was calculated by plotting the quenching rates $Q_{N'}$ against N' and fitting to the law $Q_{N'} = Q_0 e^{\gamma N'}$. The deviation of the quenching rates determined in this way from the directly measured values was less than 1% in all cases. The total error for Q_0 (ca. 8%) consists of the statistical error and an estimated error for the detection system. A fit to the measured Q_0 values gave the empirical expression $Q_0 = 150T^{-0.23\pm0.05}$. Errors in the temporal curves due to possible saturation effects should be insignificant for the following reason: in the case of saturation (or partial saturation), stimulated emission makes a certain finite contribution to the depopulation of the excited state. However, this effect only occurs during the laser pulse and all lifetimes are evaluated *after* the pulse has decayed.

Figure 2 shows Q_0 as a function of temperature; the decrease in Q_0 is only 17% over the entire region (spanning a temperature range of 1023–2285 K) and is thus consistent with studies on individual collisional partners [20], which show that the collisional partner specific cross sections in general vary only slightly in this temperature range. The five stable collisional partners H_2O, CO_2, CO, H_2, and O_2, (87.4% of all species in the burnt gas region of the flame contribute about 80% to the total quenching rate in the burnt gases. The other 20% of the quenching effect has to come from collisions with radicals (H, O, OH). In comparison, at ~ 1500 K (according to the model calculation [24]) the radicals make up only 3% of all species.

At heights of 3 and 30 mm above the burner head, i.e. at flame temperatures of 1272 K and 2234 K respectively, the collisional rates following excitation of various rotational transitions were determined. Figure 3 shows the dependence of quenching rate on the rotational quantum number N' of the excited state. The full line gives the fit of values to the empirical equations:

$$Q_{1272\,\mathrm{K}} \propto \mathrm{e}^{-(0.056\pm0.007)N'},$$
$$Q_{2234\,\mathrm{K}} \propto \mathrm{e}^{-(0.015\pm0.004)N'}.$$

At 30 mm (2234 K), the total quenching rate decreases only 19% from $N' = 0$ to 15. At 3 mm (1272 K), in contrast, the corresponding decrease is ca. 60%. This large difference can hardly be the result of temperature dependencies of the individual quenching cross sections (cf. Fig. 3 and [20]). If the gradients of the species concentrations in the flame front are considered [25], then it is seen that the fraction of H_2O at 1272 K (32%) is much smaller than at 2234 K (44.6%). On the other hand, the total fraction of H_2O, O_2, CO_2 and CO is about 80% for both temperatures. Collision partner specific investigations show [26], that the dependencies of the quenching cross sections on excited rotational quantum state for O_2, CO and CO_2 are about an order of magnitude stronger than for H_2O. Thus if the fraction of H_2O in the flame is much smaller, the rotational dependence of the total quenching effect will become correspondingly stronger. In addition, thermalization of the excited state populations at higher temperatures is much more efficient, leading to a weaker dependence of Q on N'.

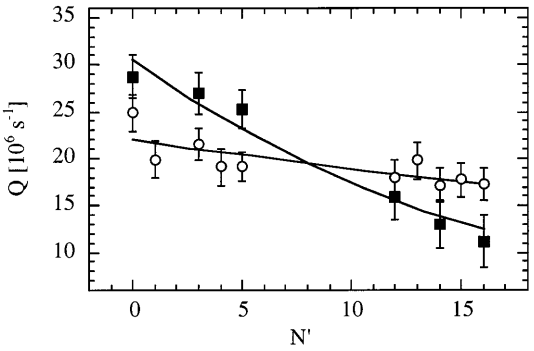

Fig. 3. Total quenching rates for OH $A^2\Sigma^+(v' = 1)$ as a function of rotational quantum number N' of the excited state ○ 2234 K, ■ 1272 K in a CH_4/O_2 flame at 10 Torr total pressure. Transitions from various branches (Q, P, R) were excited. The full curves are the fits: $Q_{1272\,\mathrm{K}} \propto \mathrm{e}^{(0.056\pm0.007)N'}$ and $Q_{2234\,\mathrm{K}} \propto \mathrm{e}^{-(0.016\pm0.004)N'}$

3.2 Vibrational energy transfer (VET)

Figure 4 shows the fluorescence spectrum for excitation of the $Q_1 5$ transition of OH $A^2\Sigma^+(v' = 1)$ at a height of 30 mm above the burner. It is seen that the fluorescence of the (0,0)-transition, compared to that of the (1,1)-transition is very weak, i.e. $\sim 6.8\%$ of the total fluorescence intensity. Therefore vibrational relaxation was, as a first approximation, neglected during simulation of the energy transfer processes. Similarly, Steffens et al. [12], on exciting the $Q_1 4$ transition of OH $A^2\Sigma^+(v' = 3)$ in a CH_4/O_2-flame at 14 Torr, found 88% of the fluorescence to be emitted from $v' = 3$ with only a few percent in each of the lower vibrational levels. On the other hand, at atmospheric pressure, vibrational transfer was found to be significant, with 47% of the emission appearing in $v' = 2$–0 for $N' = 5$ excitation. However, the amount of VET decreased with increasing rotational quantum number. In H_2/O_2-flames, which consist largely of H_2O in the burnt gas, VET was even less efficient.

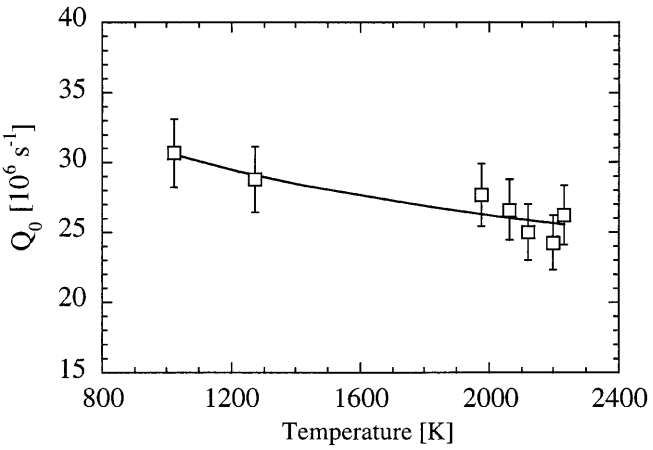

Fig. 2. Total quenching rates for OH $A^2\Sigma^+(v' = 1)$ as a function of flame temperature. The full line is the fit $Q_0 = 150T^{-0.23\pm0.05}$

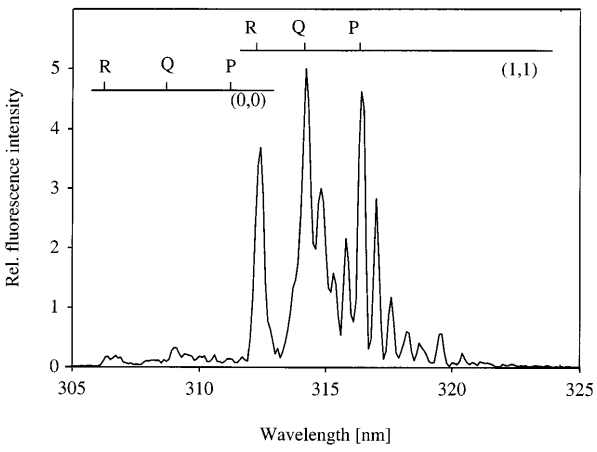

Fig. 4. Low resolution fluorescence spectrum following excitation of the $Q_1 5$-rotational transition of the OH $A^2\Sigma^+(v' = 1)$ vibrational level

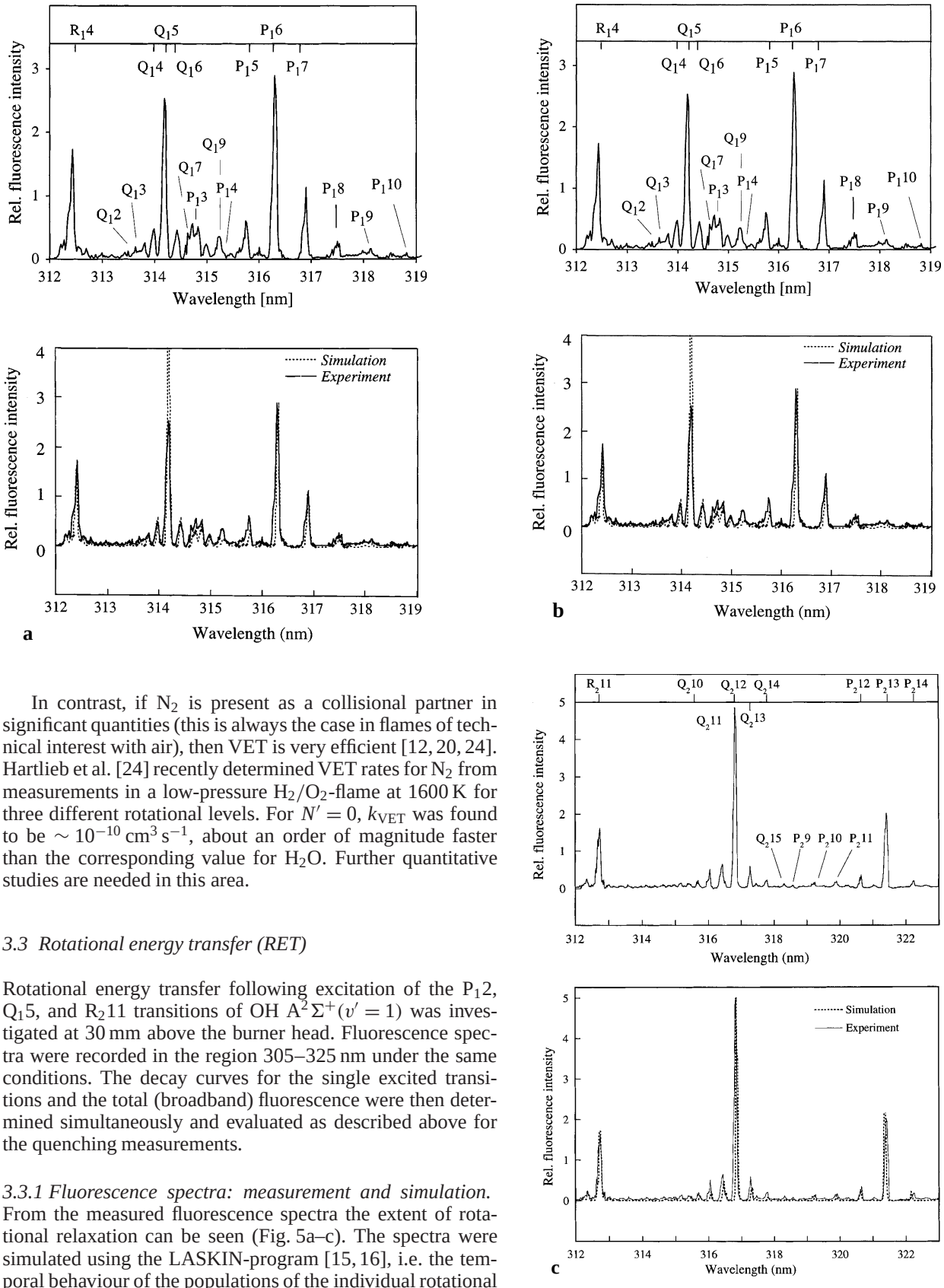

In contrast, if N_2 is present as a collisional partner in significant quantities (this is always the case in flames of technical interest with air), then VET is very efficient [12, 20, 24]. Hartlieb et al. [24] recently determined VET rates for N_2 from measurements in a low-pressure H_2/O_2-flame at 1600 K for three different rotational levels. For $N' = 0$, k_{VET} was found to be $\sim 10^{-10}$ cm^3 s^{-1}, about an order of magnitude faster than the corresponding value for H_2O. Further quantitative studies are needed in this area.

3.3 Rotational energy transfer (RET)

Rotational energy transfer following excitation of the $P_1 2$, $Q_1 5$, and $R_2 11$ transitions of OH $A^2\Sigma^+(v' = 1)$ was investigated at 30 mm above the burner head. Fluorescence spectra were recorded in the region 305–325 nm under the same conditions. The decay curves for the single excited transitions and the total (broadband) fluorescence were then determined simultaneously and evaluated as described above for the quenching measurements.

3.3.1 Fluorescence spectra: measurement and simulation. From the measured fluorescence spectra the extent of rotational relaxation can be seen (Fig. 5a–c). The spectra were simulated using the LASKIN-program [15, 16], i.e. the temporal behaviour of the populations of the individual rotational levels was calculated. The calculated values of the populations were then integrated over the time span set by the experimental temporal window of the boxcar integrators. The result was then multiplied by the fluorescence yield. The

Fig. 5a–c. Fluorescence spectrum following excitation of the OH $A^2\Sigma^+$ $(v' = 1)$ level of various rotational transitions at a height of 30 mm above the burner head. **a** $P_1 2$; **b** $Q_1 5$; **c** $R_2 11$. The upper spectrum in each pair is the measured spectrum; the lower figure shows the simulation superimposed on the experimental spectrum

discrete fluorescence intensities so obtained were then fitted to a Gauss profile, which simulated the monochromator resolution. The Gauss form was chosen as a reasonable approximation since at a temperature of ~ 2000 K, for wavelengths around 315 nm and effective excited state lifetimes of ~ 50 ns, the Doppler width is calculated to be 10.16 GHz compared to the collisional width of 3.18 GHz.

Figure 5a shows fluorescence spectra following excitation of the $P_1 2$-line. The ratio of fluorescence from the $F_1(1)$-level (sum of $P_1 2$ and $Q_1 1$) to the total fluorescence was determined to be 0.41. The simulation fluorescence spectra reproduces the measured spectral intensity profile well (Fig. 4b). The fine structure symmetry of the excited state is to a large extent conserved, i.e. predominantly F_1-F_1-transitions occur. A similar degree of symmetry conservation was observed by Stepowski and Cottereau [14] in LIF-spectra of OH $A^2\Sigma^+(v' = 0)$ in a C_3H_8/O_2-flame. A distinct preference for symmetry conservation was also seen in collision partner specific RET-measurements for collisions with H_2O [22].

In the case of $Q_1 5$ excitation (Fig. 5b), the ratio of the measured fluorescence from the $F_1(5)$ level (sum of $R_1 4$, $Q_1 5$, and $P_1 6$) to the total fluorescence was 0.44. A comparison of the measured fluorescence spectra with the simulation, showed that the intensity of the measured $Q_1 5$-line was about 45% smaller than the calculated intensity. There are two possible reasons for this discrepancy. On the detection side, a spectrally narrowband detection with any kind of polarising elements in the optical path e.g. grating of the monochromator, can lead to different ratios of the observed line intensities (especially of the *Q*-branch) depending on the way the polarisation vectors on the detection and excitation side are placed relative to one another. Furthermore, since the laser is linearly polarised and only partial depolarisation will have occurred due to collisions, this may lead to different intensities for rotational lines affected in this way. Doherty and Crosley [27] investigated such effects in CH_4/O_2-flames diluted with N_2, Ar or He. Significant changes in the ratios of line intensities were observed for excitation of *Q* lines with the direction of fluorescence polarisation relative to that of the laser excitation, while for *P* lines the effect was much less pronounced. Polarisation effects and depolarising collisions were not included in the simulation program available to us and therefore could not be accounted for in the modelling. For recent investigations on depolarising collisions the reader is referred e.g. to [28–30].

For the $R_2 11$ transition(Fig. 5c), the RET to neighbouring levels is considerably weaker than for the other two transitions; the ratio of fluorescence from the $F_2(12)$ level (sum of $R_2 11$, $Q_2 12$, and $P_2 13$) to the total fluorescence was 0.63. Again, fine structure symmetry of the excited states is preferentially conserved and the simulation reproduces the measured spectra well.

3.3.2 RET-rates. The basis of the simulation model is a three-level system [14] with the lower and upper laser coupled levels 1 and 2 and a bath "level" 3, that which represents collectively all levels in the excited state that are populated by RET. From the measured, time-resolved intensity curves of the broadband fluorescence (corresponding to the total population $N_2 + N_3$ of the excited state) and narrow band fluorescence (corresponding to the population of the

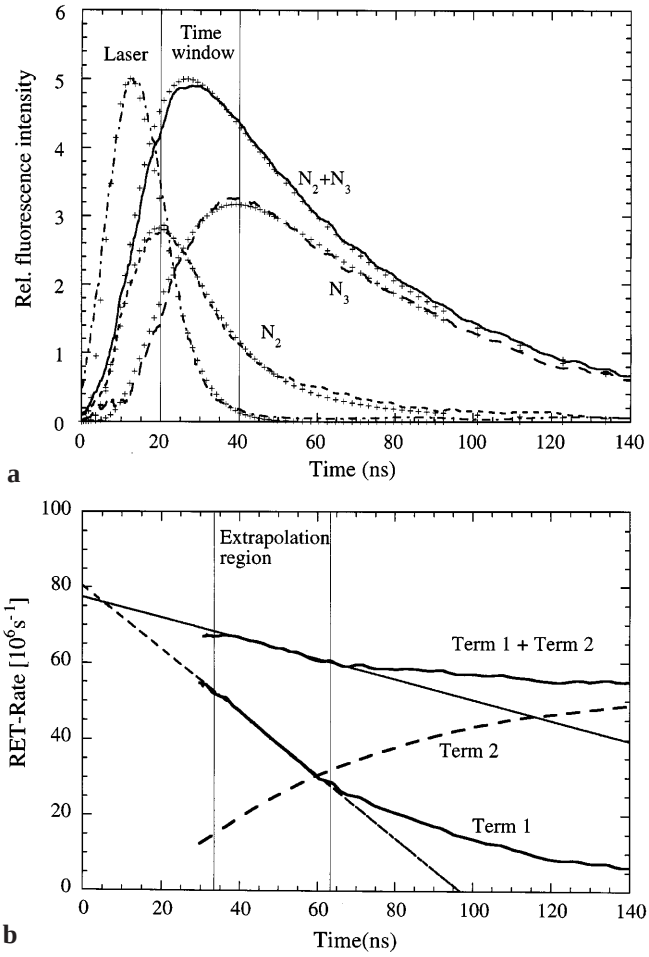

Fig. 6a,b. **a** Temporal variation of the laser pulse, total (broadband) fluorescence ($N_2 + N_3$), narrowband (single rotational line) fluorescence N_2 of the $Q_1 5$-transition and their difference N_3 (—), compared to the corresponding simulated curves (+++). **b** Determination of the RET-rate from the data of **a** by back-extrapolation, as described in the text

excited rotational transition N_2), the RET-rates can be determined as follows. Using the ratio of the fluorescence from the single excited lines to the total fluorescence (as determined above), the two time-resolved curves N_2 and $(N_2 + N_3)$ can be calibrated, whereby the ratio of the time-integrated curves has to correspond to this fluorescence ratio. The integration times are determined by the time window of the boxcar on recording the fluorescence spectrum. Subtraction of the two curves gives the temporal behaviour of N_3 (population of rotational levels in the $A^2\Sigma^+$ state populated by RET). The corresponding time decays for N_2, N_3 and $(N_2 + N_3)$ are shown in Fig. 6a for the case of $F_1(5)$ excitation, together with those from the simulation using the LASKIN-program. The comparison shows that the simulation reproduces the experimental results well. Similarly good agreement was obtained for the other two rotational lines.

The determination of the total RET-rate of the excited level follows from (4), obtained by integrating the rate equation for the bath level. The first term on the right describes the transfer rate into the bath level 3, the other two terms describe the depopulation of the bath level by electronic decay to the ground state 1 or back transfer to the laser excited level 2.

$$R_{23} = \frac{N_3(t)}{\int_0^t N_2(t')\,\mathrm{d}t'} + \frac{T_{31}\int_0^t N_3(t')\,\mathrm{d}t'}{\int_0^t N_2(t')\,\mathrm{d}t'} + \frac{R_{32}\int_0^t N_3(t')\,\mathrm{d}t'}{\int_0^t N_2(t')\,\mathrm{d}t'} \quad (8)$$

Term 1 Term 2 Term 3

For short times, the transfer from the excited level 2 into the bath level 3 dominates, while the electronic decay of the bath level only becomes significant after some time. If the population of N_3 (normalised by the integrated population for N_2) is plotted against time and then the curve extrapolated to $t = 0$, the RET-rate is obtained (Fig. 6b). However, the electronic decay $T_{31} = (A_{31} + Q_{31})$ has to be accounted for; this requires a correction of max. 10%. The RET-rate for the back transfer from the bath level is not known exactly, but for very short times can be neglected.

The RET-rates determined from the extrapolation can be converted to an effective global RET cross section by calculating an average relative velocity, whereby H_2O, CO_2 and CO are considered as collision partners of OH. The results for the RET rates and the corresponding cross sections are given in Table 1. The total error limits are obtained from the errors in the extrapolation and the errors in recording the temporal decay of the excited line.

A few other studies have been performed on rotational relaxation in flames. In the first, cross sections were measured for $N' = 1$–10, $v' = 0$ excitation in a $H_2/O_2/N_2$-Flame at 30 Torr [19]. Values obtained were in the range 110–190 Å^2, but because of the large error limits, no significant dependence on N' could be established. In the more recent work of Lee et al. on OH($v' = 0$) in a 19 Torr H_2/O_2/He-flame [15], the efficiency of RET for $N' \geq 10$ decreases significantly. The values for $N' = 1$ and 5 are the same within the error limits. The values obtained for the total RET-rates (in $10^6\,\mathrm{s}^{-1}$) were $F_1(0)$: 128 ± 32, $F_2(5)$: 108 ± 9, $F_2(12)$: 65 ± 13. These values are larger than those obtained in the CH_4/O_2-flame, where both CO_2 and H_2O are major collision partners, but the RET efficiencies for CO_2 are generally significantly lower than those of H_2O [22]. In contrast, in hydrogen flames, H_2O is mainly responsible for RET.

Finally, for OH ($v' = 2$) excitation in an atmospheric pressure flame, Bormann et al. [10] calculated an RET rate of $2.88 \times 10^9\,\mathrm{s}^{-1}$ for excitation of $J'' = 12.5$. This translates to $37.4 \times 10^6\,\mathrm{s}^{-1}$ at 10 Torr. Considering the somewhat different composition in the two flames (e.g. the H_2O-mole fraction was 13% lower in the atmospheric pressure flame), this result can be considered fairly comparable with our value of $54 \times 10^6\,\mathrm{s}^{-1}$ for a high value of N'.

With the values reported for the quenching rates in the CH_4/O_2-flame, the corresponding ratios Q/R can be calculated (Table 1). The ratio Q/R is primarily determined by the RET-rate, since the quenching rates at 2234 K vary only slightly with rotational quantum number. An even stronger increase in the Q/R ratio can be seen in [28] for a CH_4/air-flame ($v' = 0$)-excitation, where Q/R varies from 0.11 to 0.32 in the range $N' = 0$–16.

Table 1. Total RET rates following excitation of OH ($v' = 1$)

Excited transition	N'	RET-rate $R_{23}[10^6\,\mathrm{s}^{-1}]$	σ_{RET} [Å^2]	Q/R
$P_1 2$	1	89 ± 10	125 ± 14	0.22
$Q_1 5$	5	77 ± 7	109 ± 11	0.25
$R_2 11$	12	54 ± 8	76 ± 11	0.33

Acknowledgements. This work was supported by the Deutsche Forschungsgemeinschaft (Project No. 469/6-1). We also thank the Institut für Physikalische Chemie der Verbrennung/DLR (Stuttgart) for making the LASKIN-Programm available and Prof. K. Kohse-Höinghaus and colleagues for making results of their work ([24]) available prior to publication.

References

1. M. Köllner, P. Monkhouse, J. Wolfrum: Chem. Phys. Lett. **168**, 355 (1990)
2. R. Schwarzwald, P. Monkhouse, J. Wolfrum: 22nd Symposium (International) on Combustion (The Combustion Institute 1988) p. 1413
3. M. Köllner, P. Monkhouse: Appl. Phys. B **61**, 499 (1995)
4. A. Dreizler, R. Tadday, P. Monkhouse, J. Wolfrum: Appl Phys. B **57**, 85 (1993)
5. T.A. Reichardt, M.S. Klassen, G.B. King, N.M. Laurendeau: Appl. Opt. **34**, 973 (1995)
6. M.S. Klassen, T.A. Reichardt, G.B. King, N.M. Laurendeau: Combust. Sci. Technol. **97**, 391 (1994)
7. S. Agrup, M. Aldén: Opt. Commun. **113**, 315 (1994)
8. S. Agrup, M. Aldén: Appl. Spectrosc. **48**, 1118 (1994)
9. S. Agrup, F. Ossler, M. Aldén: Appl. Phys. B. **61**, 479 (1995)
10. F. Bormann, T. Nielsen, M.D. Burrows, P. Andresen: Appl. Phys. B **62**, 601 (1996)
11. M. Tsujishita, A. Hirano: Appl Phys. B **62**, 255 (1996)
12. K.L. Steffens, J.B. Jeffries, D.R. Crosley: Opt. Lett. **18**, 1355 (1993)
13. R.J. Cattolica, T.G. Mataga: Chem. Phys. Lett. **182**, 623 (1991)
14. D. Stepowski, M.-J. Cottereau: Combust. Flame **40**, 65 (1981); J. Chem. Phys. **74**, 6674 (1981)
15. M. Lee, R. Kienle, K. Kohse-Höinghaus: Appl. Phys. B **58**, 447 (1994)
16. M. Lee, R. Kienle, K. Kohse-Höinghaus: Appl. Phys. B **62**, 583 (1996)
17. K. Kohse-Höinghaus, J.B. Jeffries, R.A. Copeland, G.P. Smith, D.R. Crosley: 22nd Symposium (International) on Combustion (The Combustion Institute 1988) p. 1857
18. J. Fitzer: Diplomarbeit, Universität Heidelberg (1993)
19. R.P. Lucht, D.W. Sweeney, N.M. Laurendeau: Appl. Opt. **25**, 4086 (1986)
20. G.P. Smith, D.R. Crosley: Appl. Opt. **22**, 1428 (1983)
21. P.H. Paul, J.L. Durant, Jr., J.A. Gray, M.R. Furlanetto: J. Chem. Phys. **102**, 8378 (1995); P.H. Paul: J. Phys. Chem. **99**, 8472 (1995)
22. A. Jörg, U. Meier, K. Kohse-Höinghaus: J. Chem. Phys. **93**, 6453 (1990); A. Jörg, U. Meier, R. Kienle, K. Kohse-Höinghaus: Appl. Phys. B **55**, 304 (1992); A. Jörg, R. Kienle, K. Kohse-Höinghaus: Appl. Phys. B **56**, 249 (1993)
23. M. Lee, R. Kienle, K. Kohse-Höinghaus: Appl. Phys. B **62**, 185 (1996)
24. T. Hartlieb, D. Markus, W. Kreutner, K. Kohse-Höinghaus: Appl. Phys. B **65**, 81 (1997)
25. P. Klaus/IWR, Universität Heidelberg, Flame calculation according to the mechanism of J. Warnatz: Ber. Bunsen-Ges. Phys. Chem. **82**, 193, 643, 834 (1978); **83**, 950 (1979), adapted for the CH_4/O_2-Flamme von C. Chevalier: Ph.D. Thesis, Heidelberg University (1992)
26. R.A. Copeland, M.J. Dyer, D.R. Crosley: J. Chem. Phys. **83**, 4022 (1985)
27. P.M. Doherty, D.R. Crosley: Appl. Opt. **23**, 713 (1984)
28. S. Williams, L.A. Rahn, R.N. Zare: J. Chem. Phys. **104**, 3947 (1996)
29. R. Tadday, A. Dreizler, A.A. Suvernev, T. Dreier: Chem. Phys. Lett. **240**, 315 (1996)
30. W. Schade, J. Walewski, A. Offt, A. Knack: Phys. Rev. **53**, R2921 (1996)
31. G.P. Smith, D.R. Crosley: 18th Symposium (International) on Combustion (The Combustion Institute 1981) p. 1511